

Co-Optimization of EV Charging Control and Incentivization for Enhanced Power System Stability

Amit Kumer Podder, Tomonori Sadamoto, and Aranya Chakraborty

Abstract—We study how high charging rate demands from electric vehicles (EVs) in a power distribution grid may collectively cause its dynamic instability, and, accordingly, how a price incentivization strategy can be used to steer customers to settle for lesser charging rate demands so that these instabilities can be avoided. We pose the problem as a joint optimization and optimal control formulation. The optimization determines the optimal charging setpoints for EVs to minimize the \mathcal{H}_2 -norm of the transfer function of the grid model, while the optimal control simultaneously develops a linear quadratic regulator (LQR) based state-feedback control signal for the battery-currents of those EVs to jointly minimize the risk of grid instability. A subsequent algorithm is developed to determine how much customers may be willing to sacrifice their intended charging rate demands in return for financial incentives. Results are derived for both unidirectional and bidirectional charging, and validated using numerical simulations of multiple EV charging stations in the IEEE 33-bus power distribution model.

Index Terms—Electric vehicles, charging control, price incentivization, co-optimization, voltage stability, LQR

NOMENCLATURE

$\mathbb{N}_P, \mathbb{N}_E, \mathbb{N}_L$	index set of point of common coupling (PCC) bus, EVCS bus, and non-EVCS load bus
V_k	k^{th} bus voltage phasor. Let V_k^d and V_k^q be the d-q axis voltage.
$\mathcal{C}^{PD}, \mathcal{C}^{P*}$	charging/discharging price at the demanded and optimal charging/discharging power rate
$\mathcal{C}^{tD}, \mathcal{C}^{t*}$	charging/discharging duration at the demanded and optimal charging/discharging power rate
$\mathcal{W}^t, \mathcal{I}^e$	waiting time and dollar incentives
E^D	energy demand vector from EVs
n	number of bus
p	number of EVCS
P^{e*}, i^{e*}	optimal charging power and current vector
P^{eD}, i^{eD}	demanded charging power and current vector
P_k^L, Q_k^L	non-EVCS load at k^{th} bus

Mathematical Notations: We denote the sets of real and complex numbers by \mathbb{R} and \mathbb{C} , respectively. $j := \sqrt{-1}$. $\mathbf{1}_n := [1, \dots, 1]^T \in \mathbb{R}^n$. Given $x_{k_1}, \dots, x_{k_w} \in \mathbb{R}^{1 \times N}$ and $\mathcal{K} := \{k_1, \dots, k_w\}$, the quantity $[x_k]_{k \in \mathcal{K}} := [x_{k_1}, \dots, x_{k_w}] \in \mathbb{R}^{1 \times wN}$. For $\mathbb{N} := \{1, \dots, n\}$, we denote the block-diagonal matrix having matrices M_1, \dots, M_n on its diagonal blocks

by $\text{diag}(M_k)_{k \in \mathbb{N}}$. For $x := [x_1, \dots, x_n]^T \in \mathbb{R}^n$ and $\beta_1, \dots, \beta_n \in \mathbb{R}$, we define $\|x\|_{2,\beta} := x^T \text{diag}(\beta_k)_{k \in \{1, \dots, n\}} x$ and $\|x\|_{\infty,\beta} := \max\{\beta_1 x_1, \dots, \beta_n x_n\}$, where $\|x\|_2 := x^T x$. We define the element-wise multiplication and division by \odot and \oslash , respectively, i.e., for $x := [x_1, \dots, x_p]^T \in \mathbb{R}^p$ and $y := [y_1, \dots, y_p]^T \in \mathbb{R}^p$, $x \odot y := [x_1 y_1, \dots, x_p y_p]^T \in \mathbb{R}^p$ and $x \oslash y := [x_1/y_1, \dots, x_p/y_p]^T$, respectively. Given $X \geq 0$, we denote its Cholesky factor $X^{\frac{1}{2}}$ such that $X = X^{\frac{1}{2}} X^{\frac{1}{2}}$. Given a stable strictly proper transfer matrix $G(s)$, its \mathcal{H}_2 -norm is defined as $\|G(s)\|_{\mathcal{H}_2} := \left(\frac{1}{2\pi} \int_{-\infty}^{\infty} \text{tr}(G(j\omega)G^T(j\omega)) d\omega \right)^{\frac{1}{2}}$ where tr is the trace operator. For any symbol \bullet , we denote its setpoint as \bullet^* . For three vectors x_1, x_2, x_3 of same dimension, $x_1 \in [x_2, x_3]$ means each element of x_1 is lower and upper bounded by the corresponding elements of x_2 and x_3 .

I. INTRODUCTION

ELECTRIC vehicles (EVs) are envisioned to be an integral component for achieving nationwide goals of reducing greenhouse gas emissions and carbon footprint in the United States (US) over the foreseeable future. A significant amount of research has already been done over the last decade on how charging of EVs should be priced cost-effectively for both EV drivers and the owners of the charging stations as well as the local utility companies, considering various factors such as locations of the charging stations, traffic patterns in the neighborhoods under consideration, range anxiety, demographic factors, and locational marginal pricing of electricity during various hours of the day [1]–[4]. Pricing includes electricity costs based on actual consumption and a portion of fixed costs for operations and maintenance of the stations such as connection fees. The price range may vary depending on the amount of energy requested by the driver, and the time frame the driver allows the charging port of the electric vehicle charging station (EVCS) to deliver that energy. Software-defined apps have been developed to estimate and display the total session fees when users enter their charging demand information in the app. The exact rate paid per charging session is based on the actual amount of energy received.

However, one critical issue that has been paid far less attention to is how charging controls and their associated pricing may adversely impact the dynamical characteristics and stability of the distribution grid from where the EVs are drawing power. For instance, if the number of EVs in the US increases exponentially over the next decade, and if EV owners keep following the same charging control and pricing mechanisms as now, will that encourage a large fraction of drivers to charge their cars at certain specific times of the day

This work was supported in part by the US National Science Foundation under grant ECCS 1931932.

A. Podder and A. Chakraborty are with the Department of Electrical and Computer Engineering, North Carolina State University, Raleigh, NC 27606. Emails: {apodder, achakra2}@ncsu.edu

T. Sadamoto is with the Department of Mechanical Engineering and Intelligent Systems, The University of Electro-Communications, Chofugaoka, Chofu, Tokyo. Email: sadamoto@uec.ac.jp

thereby causing overloading problems in the grid, resulting in poor damping of small-signal oscillations, or even voltage instability? More constructively speaking, are there ways by which grid operators may be able to incentivize EV customers to settle for a slightly lesser charging power rate than what they desire for the same charging duration, or equivalently for a slightly longer charging duration for the same energy demand, and thereby control charging patterns across neighborhoods or cities such that instability issues in the local distribution grid can be prevented?

This paper presents a co-optimization approach to address this open question. Stability analysis of power distribution networks with EV charging has been addressed in several recent papers. For example, the studies in [5], [6] identify the interconnection structure between an EVCS and a DC distribution network, and other network parameters and topology as the primary factors affecting small-signal stability. Results in [7] introduce a comprehensive small-signal dynamic model for DC fast charging stations that encompasses both islanded mode and grid-connected mode, showing the impacts of PI-based charging controllers on dominant eigenvalues. But the end goal of all of these designs is to improve steady-state regulation of the charging setpoints, and not the dynamic performance of the system states. Moreover, there is also no study that quantifies the direct correlation between pricing, control design, and closed-loop dynamics. To resolve this issue, we first develop a detailed dynamical model of the distribution grid with multiple EVCSs and show how the conventional PI-control-based current controllers in their power electronic circuits can easily result in poor damping responses when the EV load is high. We formulate a joint optimization and optimal control problem, where the optimization determines the optimal charging set points of the EVs to improve small-signal damping by minimizing the \mathcal{H}_2 -norm of the grid transfer function while the optimal control part simultaneously designs a linear quadratic regulator (LQR)-based state feedback law for the battery currents to jointly minimize the risk of grid instability. A subsequent algorithm is developed to determine how much customers may be willing to sacrifice their intended charging durations in return for financial incentives. The algorithm can be implemented in the form of an app where EV drivers can submit their charging demands ahead of time to explore the possibilities of discounted rates. The algorithm is also extended to demonstrate the trade-off between price, small-signal stability, and voltage stability of the grid when the EVCSs operate in bidirectional charging mode. Results are validated using numerical simulations of the modified IEEE 33-bus radial distribution system model with multiple EVCSs. The benefits and drawbacks of the proposed controller on the closed-loop time response of the grid are reported.

The rest of the paper is organized as follows. Section II recapitulates the nonlinear state-space model of a distribution grid. Section III presents a motivating example to show how continued growth in EV penetration may worsen small-signal performance of the grid states. Section IV presents the problem formulation and main results, first for a simplified EVCS model with unidirectional charging, and thereafter for a more generalized model with both uni- and bidirectional

charging. Section IV describes the practical implementation of the proposed algorithm, followed by numerical results in Section V. Section VI concludes the paper.

II. MODEL OF EVCS INTEGRATED POWER SYSTEM

We consider a n -bus power distribution model. Without loss of generality, let Bus 1 be the point of common coupling (PCC) of the distribution side with the bulk transmission grid, which for this model is simply modeled as a constant high voltage source. The non-EVCS loads are modeled as constant PQ-loads that consume constant real power P_k^L and constant reactive power Q_k^L for the k^{th} load, $k \in \mathbb{N}_L$. We consider the d - q axis formulation of power flow. We assume the distribution grid topology to follow a radial line network. This assumption is, however, only for simplicity of the model, and does not impact our proposed optimization or control design. The same design will be applicable if the grid topology follows a meshed network. The d - q axis admittance of the line connecting the k^{th} bus and the h^{th} bus, $k = 1, \dots, n-1$, is denoted as $G_{kh}^{dq} + jB_{kh}^{dq} \in \mathbb{C}^2$, for any $h \in \mathcal{N}_k$, where \mathcal{N}_k is the set of neighboring buses to the k^{th} bus, where the conductance vector $G_{kh}^{dq} := [G_{kh}^d, G_{kh}^q]^\top$, and the susceptance vector $B_{kh}^{dq} := [B_{kh}^d, B_{kh}^q]^\top$. The conventional EVCS configuration is considered, as shown in Fig. 1, which consists of a centralized AC/DC converter with a front-end LCL filter for creating a common DC bus, and DC/DC converters, which act as the charging ports. For more details about the model, please see [8].

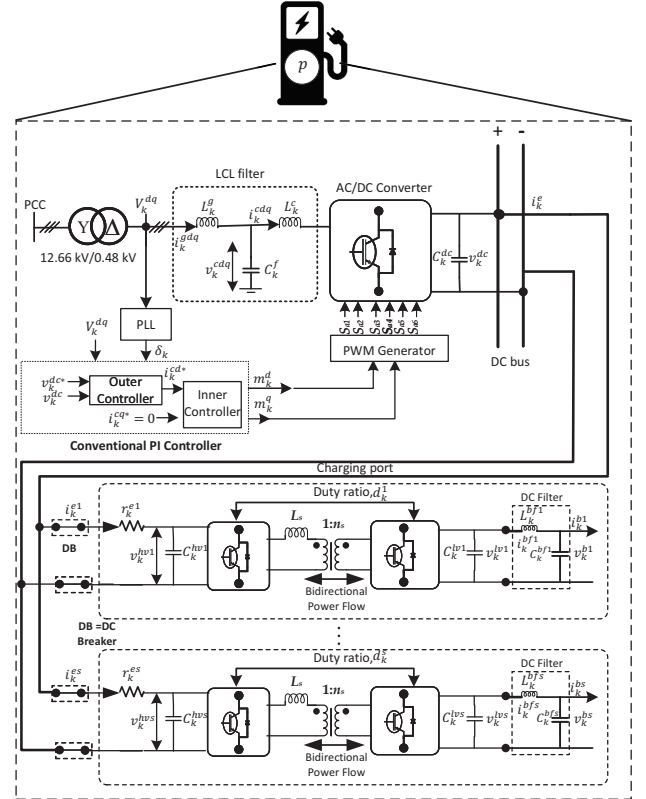


Fig. 1. Generalized diagram for an EVCS and its internal dynamic components.

The synchronization between the EVCS and the network is ensured by a type-2 synchronous reference frame PLL,

TABLE I
PLL AND AC/DC CONVERTER FILTER DYNAMICS OF p EVCSs, $k \in \mathbb{N}_E$

Phase locked loop (PLL) dynamics:	
$\begin{cases} \dot{\delta}_k = \bar{\omega}(\omega_k - \omega_c) \\ \zeta_k = \kappa_k^{I1}(V_k^q - 0), \quad \omega_k = \kappa_k^{P1}(V_k^q - 0) + \zeta_k \end{cases} \quad (1)$	
where, δ_k , ω_k , $\bar{\omega}$, and ω_c are the synchronous phase angle, angular frequency, base angular frequency, and common angular frequency, respectively. ζ_k is the intermediate state variable of the PLL, and κ_k^{P1} and κ_k^{I1} are the proportional-integral (PI) gains of the PLL.	
AC/DC converter with LCL filter dynamics:	
$\begin{cases} L_k^g i_k^{gd} = V_k^d - v_k^{cd} + \omega_k L_k^g i_k^{gq} \\ L_k^g i_k^{gq} = V_k^q - v_k^{cq} - \omega_k L_k^g i_k^{gd} \end{cases} \quad (2)$	
$\begin{cases} C_k^f i_k^{cd} = i_k^{gd} - i_k^{cd} + \omega_k C_k^f v_k^{cq} \\ C_k^f v_k^{cq} = i_k^{gq} - i_k^{cq} - \omega_k C_k^f v_k^{cd}, \end{cases} \quad (3)$	
$\begin{cases} L_k^c i_k^{cd} = v_k^{cd} - \frac{m_k^d v_k^{dc}}{2} + \omega_k L_k^c i_k^{cq} \\ L_k^c i_k^{cq} = v_k^{cq} - \frac{m_k^q v_k^{dc}}{2} - \omega_k L_k^c i_k^{cd} \end{cases} \quad (4)$	
where, L_k^g , C_k^f , and L_k^c are the LCL filter parameters, m_k^d and m_k^q are the d - q axis duty cycles, v_k^{dc} is the DC link voltage, V_k^d and V_k^q are the d - q axis components of the input bus voltage, i_k^{gd} and i_k^{gq} are the d - and q -axis input side filter currents, v_k^{cd} and v_k^{cq} are the voltages across the filter capacitor, and i_k^{cd} and i_k^{cq} are converter side filter currents, respectively.	

TABLE II
CONVERTER CONTROLLER & DC BUS DYNAMICS OF p EVCSs, $k \in \mathbb{N}_E$

Outer control loop:	
$\begin{cases} \dot{\Psi}_k = \kappa_k^{I2}(v_k^{dc*} - v_k^{dc}) \\ i_k^{dc*} = \kappa_k^{P2}(v_k^{dc*} - v_k^{dc}) + \Psi_k, \quad i_k^{cq*} = 0 \end{cases} \quad (5)$	
Inner control loop:	
$\begin{cases} \dot{\chi}_k^d = \kappa_k^{I3}(i_k^{cd*} - i_k^{cd}) \\ m_k^d = \text{sat} \left(\frac{2}{v_k^{dc}} (\kappa_k^{P3}(i_k^{cd*} - i_k^{cd}) + \chi_k^d + \tilde{V}_k^d) + \Delta m_k^d \right) \end{cases} \quad (6)$	
$\begin{cases} \dot{\chi}_k^q = \kappa_k^{I4}(i_k^{cq*} - i_k^{cq}) \\ m_k^q = \text{sat} \left(\frac{2}{v_k^{dc}} (\kappa_k^{P4}(i_k^{cq*} - i_k^{cq}) + \chi_k^q + \tilde{V}_k^q) + \Delta m_k^q \right), \end{cases} \quad (7)$	
where, Ψ_k is the internal state variable of the outer loop, and χ_k^d and χ_k^q are the internal state variables of the inner loop controllers, respectively. κ_k^{P2} , κ_k^{I2} , κ_k^{P3} , κ_k^{I3} , κ_k^{P4} , and κ_k^{I4} are the PI gains of the outer and inner loop controllers. $\tilde{V}_k^d = \omega_k L_k i_k^{cq} + V_k^d$, $\tilde{V}_k^q = V_k^q - \omega_k L_k i_k^{cd}$, and $L_k = L_k^g + L_k^c$. Δm_k^d and Δm_k^q are the controllable inputs, and $\text{sat}(\cdot)$ is the saturation function between $[-1, 1]$.	
DC bus dynamics:	
$\dot{v}_k^{dc} = \frac{3(m_k^d i_k^{cd} + m_k^q i_k^{cq})}{2C_k^{dc}} - \frac{i_k^{e*} + \Delta i_k^e}{C_k^{dc}}, \quad (8)$	
where, C_k^{dc} is the DC link capacitance, i_k^{e*} is the charging current setpoint, and Δi_k^e is the controllable charging current.	

which provides the synchronous phase angle (δ_k , $k \in \mathbb{N}_E$) required for designing the controller of the converter. The dynamics of the PLL and the AC/DC converter with LCL filter are presented in Table I. The conventional PI-based controller is used for the converter and the dynamics of the converter controller and DC bus are shown in Table II. Each EVCS may have multiple charging ports connected to their respective DC buses, where every charging port has similar internal dynamics [7]. The dynamics of the charging ports are ignored for simplicity as their time scale is significantly faster than that of the grid state variables that we are interested in.

TABLE III
LINE DYNAMICS AND POWER BALANCE

Line dynamics For $k = \{1, \dots, n-1\}$, and $h \in \mathcal{N}_k$	
$\begin{cases} \dot{i}_{kh}^d = \frac{1}{l_{kh}} (V_k^d - V_h^d + \frac{G_{kh}^d \omega_c l_{kh}}{B_{kh}^d} i_{kh}^d + \omega_c l_{kh} i_{kh}^q) \\ \dot{i}_{kh}^q = \frac{1}{l_{kh}} (V_k^q - V_h^q + \frac{G_{kh}^q \omega_c l_{kh}}{B_{kh}^q} i_{kh}^d i_{kh}^q - \omega_c l_{kh} i_{kh}^d), \end{cases} \quad (9)$	
where, i_{kh}^d and i_{kh}^q are the d - q axis branch currents. l_{kh} is the line reactance.	
Power balance	
At PCC, i.e., for $k \in \mathbb{N}_P$,	
$\begin{cases} P_k^g = \frac{3}{2} \left(\sum_{h \in \mathcal{N}_k} V_k^d V_h^d G_{kh}^d + \sum_{h \in \mathcal{N}_k} V_k^q V_h^q G_{kh}^q \right) \\ Q_k^g = \frac{3}{2} \left(\sum_{h \in \mathcal{N}_k} V_k^q V_h^d B_{kh}^d - \sum_{h \in \mathcal{N}_k} V_k^d V_h^q B_{kh}^q \right). \end{cases} \quad (10)$	
For $k \in \mathbb{N}_L, \mathbb{N}_E$,	
$\begin{cases} P_k^L + P_k^e = \frac{3}{2} \left(\sum_{h \in \mathcal{N}_k} V_k^d V_h^d G_{kh}^d + \sum_{h \in \mathcal{N}_k} V_k^q V_h^q G_{kh}^q \right) \\ Q_k^L + Q_k^e = \frac{3}{2} \left(\sum_{h \in \mathcal{N}_k} V_k^q V_h^d B_{kh}^d - \sum_{h \in \mathcal{N}_k} V_k^d V_h^q B_{kh}^q \right) \end{cases} \quad (11)$	
where,	
$P_k^e = \frac{3}{2} (V_k^d i_{kh}^{gd} + V_k^q i_{kh}^{gq}), \quad Q_k^e = \frac{3}{2} (V_k^q i_{kh}^{gd} - V_k^d i_{kh}^{gq}). \quad (12)$	
P_k^g and Q_k^g in (10) are the active and reactive power generated by the bulk transmission grid (modeled as a constant voltage source), P_k^L and Q_k^L in (11) are that consumed by the non-EV loads, while P_k^e and Q_k^e in (12) are that consumed by the EVs.	

This will also be verified later via an eigenvalue analysis in the motivating example in Section IV. Short-line models are considered for the interconnecting tie-lines between the buses. The line dynamics and power flow using d - q axis components are presented in Table III. The overall state-space model of the EVCS-integrated power system can be presented in a compact form by the following differential-algebraic equations (DAEs):

$$\Sigma : \begin{cases} \dot{x} = f(x, y, u, \alpha) \\ 0 = g(x, y, \alpha) \end{cases} \quad (13)$$

where,

$$\begin{aligned} x &:= [[(x_k^e)^T]_{k \in \mathbb{N}_E}, [i_{kh}^d, i_{kh}^q]_{k \in \{1, \dots, n-1\}, h \in \mathcal{N}_k}]^T \in \mathbb{R}^{12p+2(n-1)} \\ x_k^e &:= [\delta_k, \zeta_k, i_k^{gd}, i_k^{gq}, i_k^{cd}, i_k^{cq}, v_k^{cd}, v_k^{cq}, \Psi_k, \chi_k^d, \chi_k^q, v_k^{dc}]^T \in \mathbb{R}^{12p} \\ u &:= [\Delta m_k^d, \Delta m_k^q, \Delta i_k^e]_{k \in \mathbb{N}_E}^T \in \mathbb{R}^{3p} \\ y &:= [V_k^d, V_k^q]_{k \in \{1, \dots, n\}}^T \in \mathbb{R}^{2n} \\ \alpha &:= [i_k^{e*}]_{k \in \mathbb{N}_E}^T \in \mathbb{R}^p, \end{aligned}$$

i_{kh}^d and i_{kh}^q are defined in (9), δ_k and ζ_k are in (1), i_k^{gd} and i_k^{gq} are in (2), v_k^{cd} and v_k^{cq} are in (3), i_k^{cd} and i_k^{cq} are in (4), Ψ_k is in (5), χ_k^d , χ_k^q , Δm_k^d and Δm_k^q are in (6) and (7), v_k^{dc} , Δi_k^e , and i_k^{e*} are in (8), respectively. The functions $f(\cdot)$ and $g(\cdot)$ follow from (1) to (11). The equilibrium of this model is determined by substituting $f(\cdot) = g(\cdot) = 0$, and solving for (x^*, y^*, u) . The algebraic variable y is eliminated and the model is then linearized around the equilibrium point (x^*, u^*) by Jacobian linearization to obtain a small-signal state-variable model that will be used shortly in the next section. Note that the control input u is already in the small-signal form, i.e., $u^* = 0$.

We close this section by recalling the definition of voltage stability index (VSI) that will be used shortly in the design reported in Section IV-C. The VSI represents the voltage

stability margin at any given bus of the distribution network and is defined at each receiving end bus. For a radial network, every receiving end bus only has one sending end bus (please note that the reverse may not be true as the sending end bus may provide power to multiple receiving end buses. For $h \in \{2, \dots, n\}$ (which is the index of the receiving end bus), let the ending bus index be denoted as $k_h \in \{1, \dots, n-1\}$. Following [9], we define the VSI at the h^{th} bus as

$$\mathcal{V}_h := V_{k_h}^{*4} - 4((P_h^{L*} + v_h^{dc*} i_h^{e*}) r_{kh} - Q_h^{L*} \mathcal{X}_{kh})^2 - 4((P_h^{L*} + v_h^{dc*} i_h^{e*}) r_{kh} + Q_h^{L*} \mathcal{X}_{kh}) V_h^{*2}, \quad (14)$$

where, V_{k_h} is the voltage at the corresponding sending end bus, $\mathcal{X}_{kh} := 2\pi\omega l_{kh}$ is the reactance between k^{th} and h^{th} buses, P_h^{L*} , and Q_h^{L*} are steady-state real and reactive powers consumed by the non-EV load in the network at the h^{th} bus. Note that $\mathcal{V}_h \in [0, 1]$ from the definition. The closer the VSI is to unity the less susceptible that bus is to a voltage collapse.

III. MOTIVATING EXAMPLE

Consider the IEEE 33-bus medium voltage power distribution network model, where p EVCSs are connected to the network as shown in Fig. 2. Three cases are considered to evaluate the impact of increasing the number of EVCSs in this model, namely, $p = 3, 5, 10$, with the respective EVCS-connected buses represented as $\mathbb{N}_E := \{3, 19, 5\}$, $\mathbb{N}_E := \{3, 5, 9, 19, 21\}$, $\mathbb{N}_E := \{3, 5, 9, 11, 15, 17, 19, 21, 26, 32\}$. In all cases, the EVCS capacity is assumed to be between 50 kW and 175 kW. The EVCS-integrated system is modeled as (13) including the dynamics of the dual active bridge (DAB) based charging ports [7]. Let this nonlinear detailed model be denoted as Σ_{detail} . The values of the system's parameters for a typical 50 kW EVCS are presented in the Appendix. Other relevant model parameters are considered following [10].

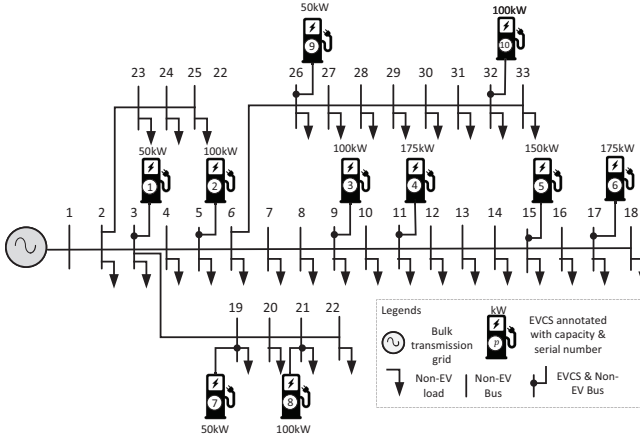


Fig. 2. IEEE 33-bus radial distribution system model with $p = 10$ EVCSs.

Fig. 3a shows the eigenvalues of the linearized model of Σ_{detail} for $p = 3$ and $p = 10$ EVCSs. It can be seen that the eigenvalues with the highest participation factor from the charging port states, the output DC filter states, and the line states (all marked in the purple region) have much faster time constants than those in the green region. We label the purple eigenvalues as “fast”, and the green eigenvalues as “dominant”.

The dominant eigenvalues show poor damping ratios. The damping worsens as the number of EVCSs increases. The transient responses of the DC bus voltage v_k^{dc} for a selected set of EVCSs, triggered by the plugging-in of their EV loads are shown in Fig. 3b. The figure shows that the voltage suffers from continued oscillations that become more severe with the increase in EV charging rates and demands. Similarly, the values of the VSI at the different buses of the network are shown in Fig. 3c. It is seen that VSI decreases with the increasing power demand from the network, i.e., with the increasing number of EVCSs. For example, with 10 EVCSs in the network, the minimum VSI and bus voltage (in bus 18) drop-down by 0.137 pu and 0.048 pu, respectively. Thus, increasing the number of EVCSs impacts both small-signal and voltage stability adversely.

In the following sections, we resolve this problem in two ways. The first approach is to request the EV customers to reduce their demand in exchange for an incentive. The challenge of achieving a balance between these incentives and the small-signal performance of the grid is discussed in Sections IV-A and IV-B. The second approach is a more comprehensive solution that takes into account not only incentivization but also leverages the bidirectional capability of EVCS to draw power from the EV batteries. This is presented in Sections IV-C and IV-D.

IV. PROPOSED ALGORITHMS

A. Problem -1: Simplified EVCS integrated grid

We assume that a central authority, referred to here onward as the central point operator (CPO), is in charge of running all the EVCSs in the grid. Let us assume that on any given day \mathcal{N}_v number of cars submit information about what time of the day they are planning to arrive at the k^{th} EVCS to charge their EVs the following day, and how much Kilo-Watt-Hour (KWhr) of energy they need for charging. Let the energy demand vector be denoted as $E^D := [E_k^D]_{k \in \mathbb{N}_E}^T \in \mathbb{R}^p$, from which the EVCS owners compute the demanded charging current rate vector $i^{eD} := [i_k^{eD}]_{k \in \mathbb{N}_E}^T \in \mathbb{R}^p$. We assume that each EVCS has a fixed capacity and only operates in grid-to-vehicle (G2V) mode, which implies that the total amount of steady-state current that the EVCSs can draw from the grid will always remain constant, irrespective of which car is coming to which port and when. In other words, for a given set of vehicles, i^{eD} is always equal to a constant number, regardless of the schedule of charging these vehicles. The demands depend on the battery specification of each specific vehicle as well as other factors depending on traffic patterns of neighborhoods, constituting the so-called *customer's objective* [3]. Our goal of this paper, in contrast, is to consider the *CPO's objective*, which is to determine the ideal value of the setpoint vector $i^{e*} := [i_k^{e*}]_{k \in \mathbb{N}_E}^T \in \mathbb{R}^p$ (which may be less than the corresponding demanded value i^{eD}) as well as to design a state-feedback controller for $u(t)$ in (13) to maximize the closed-loop damping performance of the EVCS-integrated grid against any disturbance. From the physics of power system models, it is intuitive that the grid will always have a better small-signal stability margin when i^{e*} is small versus high, i.e., when the EV loading is minimal. This indicates that the

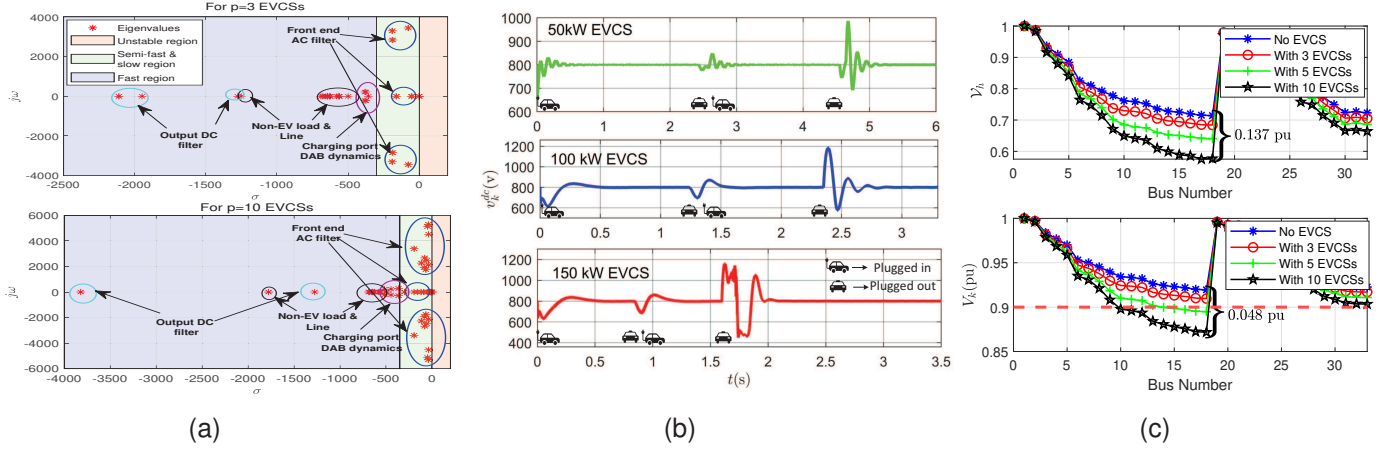


Fig. 3. (a) Open-loop eigenvalues of the linearized 33-bus distribution grid model Σ_{detail} for $p = 3$ and 10 EVCSs. (b) The transient DC bus voltage v_k^{dc} inside the 1st, 3rd, and 5th EVCSs of the EVCSs integrated systems for $p = 10$ case, respectively. Note that, the charging duration is scaled down from the real-time charging time to highlight the transients in shorter duration, and (c) Trends of VSI values of different buses of the network with the increasing number of EVCSs. The red dotted line shows the minimum allowable voltage limit in the network.

solution to the damping maximization problem will always tend towards the allowable lower bound for the demand. To avoid this problem, we add an *incentivization* term to the optimization objective that will allow customers to settle for a demand that is higher than the lowest allowable demand but lower than their desired demand i^{eD} in exchange for money. The practical implication is that the grid operator must incentivize the customers for the deficit amperes that they are sacrificing for the sake of enhancing the stability of the grid. The problem is formulated as:

$$J = \min_{K, i^{e*}} (1 - \gamma) \underbrace{\int_0^\infty \|\hat{z}\|_2^2 dt}_{J_1} + \gamma \underbrace{\|i^{e*} - i^{eD}\|_{2,\beta}^2}_{J_2} \quad (15)$$

$$\text{s.t.} \quad (13) \quad (16)$$

$$\hat{z} := Q\hat{x} + \mathcal{R}u \quad (17)$$

$$u = K\hat{x} \quad (18)$$

$$i_k^{e*} \in [\max\{i_k^{e*}, 0\}, i_k^{eD}], \quad k \in \mathbb{N}_E \quad (19)$$

where, $\hat{x} := x - x^*$, $Q := [Q^{\frac{1}{2}} \quad 0]^T$, and $\mathcal{R} := [0 \quad R^{\frac{1}{2}}]^T$, β_k is the price incentive constant, i_k^{e*} is the k -th lowest allowable demand, and \hat{z} represents the measure for quantifying the damping performance. Note that since all EVCSs are assumed to be uni-directional, the max operation is introduced into (19). The matrices $Q \geq 0 \in \mathbb{R}^{7p \times 7p}$, and $R > 0 \in \mathbb{R}^{3p \times 3p}$ are constant weight matrices that can be decided by the grid operator depending on how much damping improvement is needed versus how much control energy can be spent on the feedback. The matrix $K \in \mathbb{R}^{3p \times 7p}$ is the optimal control gain, and $\gamma \in [0, 1]$ is a normalizing factor.

B. Solution Approach of Problem 1

For a given i^{e*} , a linearized model of (13) with the performance output \hat{z} is uniquely determined as

$$G_{i^{e*}} : \begin{cases} \dot{\hat{x}} = A(i^{e*})\hat{x} + B(i^{e*})u, & \hat{x}(0) = \hat{x}_0 \\ \hat{z} = Q\hat{x} + \mathcal{R}u, \end{cases} \quad (20)$$

where Q, \mathcal{R} are defined as in (17). A relaxation strategy is used to make K uniquely determined as a function of i^{e*} as:

$$J_R = \min_{i^{e*}} (1 - \gamma) \underbrace{\|G_{i^{e*}}\|_{\mathcal{H}_2}^2}_{J_{R1}} + \gamma \underbrace{\|i^{e*} - i^{eD}\|_{2,\beta}^2}_{J_{R2}} \quad (21)$$

$$\text{s.t.} \quad (19), (20) \quad (22)$$

$$u = K(i^{e*})\hat{x} \quad (23)$$

$$K(i^{e*}) = \text{LQR}(i^{e*}), \quad (24)$$

where,

$$\text{LQR}(i^{e*}) = \min_{K(i^{e*})} \left\| \begin{bmatrix} Q^{\frac{1}{2}} \\ R^{\frac{1}{2}} \end{bmatrix} (sI - A_{cl}(i^{e*}))^{-1} \right\|_{\mathcal{H}_2}^2, \quad (25)$$

$$A_{cl}(i^{e*}) := A(i^{e*}) - B(i^{e*})K(i^{e*}) \in \mathbb{R}^{7p \times 7p}. \quad (26)$$

To find the balance of the optimal setpoint $i^{e*} \in \mathbb{R}^p$ considering the damping objective (J_{R1}) and the incentivization objective (J_{R2}), we propose a gradient-based algorithm by using the concept of minimizing the \mathcal{H}_2 -norm of a transfer function as presented in [11] with a minor modification. The procedure is summarized as follows.

The transfer function matrix $G_{i^{e*}}(s)$ in (20) with the controller in (23) for the initial state disturbance $\hat{x}(0)$ can be written as

$$G_{i^{e*}}(s) := C(sI - A_{cl}(i^{e*}))^{-1}\hat{x}_0, \quad (27)$$

where, $C := Q + \mathcal{R}K$. Let l be the iteration number and $i^{e*}(l)$ be the l -th guess of an optimal i^{e*} . Given $k \in \mathbb{N}_E$, let p_k be the number of elements in \mathbb{N}_E that are less than or equal to k (e.g., if $\mathbb{N}_E := \{3, 19, 5\}$, then $p_3 = 1, p_{19} = 2$). Under this setting, we first consider deriving a linear perturbed model of $G_{i^{e*}}$ for the decision variable i^{e*} , described as follows. Given $\epsilon > 0$, for $k \in \mathbb{N}_E$, we consider a perturbed setpoint by increasing only the p_k -th element of $i^{e*}(l)$ by ϵ , i.e.,

$$i_k^{e*}(l) := i_k^{e*}(l) + e_k^p \epsilon, \quad e_k^p := [0, \dots, 1, \dots, 0]^T \in \mathbb{R}^p. \quad (28)$$

Then, the closed-loop state matrix at this perturbed setpoint can be written as

$$A_{cl,k} := A(i_k^{e*(l)}) - B(i_k^{e*(l)})K(i_k^{e*(l)}) \quad (29)$$

where K is newly designed by (24)-(25). Therefore, by denoting the difference of the transfer function as

$$\Delta G_k := (C(sI - A_{cl,k})^{-1}\hat{x}_{0,k} - G_{i^{e*(l)}}) / \epsilon, \quad (30)$$

the linear approximation of $G_{i^{e*}}$ around $i^{e*} = i^{e*(l)}$ can be written as

$$G_{i^{e*}}(s) \approx G_{i^{e*(l)}}(s) + \sum_{k \in \mathbb{N}_E} \Delta G_k(s)\epsilon. \quad (31)$$

Define $\{A_{\Delta,k}, B_{\Delta,k}, C_{\Delta,k}\}$ such that $\Delta G_k = C_{\Delta,k}(sI - A_{\Delta,k})^{-1}B_{\Delta,k}$. Then, the RHS of (31) can be written as $\mathcal{X} = \mathcal{A}\mathcal{X} + (B_1 + B_2\epsilon\mathbf{1}_p)\delta_t$, $\hat{z} = \mathcal{C}\mathcal{X}$ where δ_t is the Dirac delta, $B := B_1 + B_2\epsilon\mathbf{1}_p$, and

$$\mathcal{A} := \text{diag}(A_{cl}(i^{e*(l)}), \text{diag}(A_{\Delta,k})_{k \in \mathbb{N}_E}), \quad (32)$$

$$B_1 := [\hat{x}_0^\top, 0]^\top, \quad (33)$$

$$B_2 := [0, \text{diag}(B_{\Delta,k}^\top)_{k \in \mathbb{N}_E}]^\top, \quad (34)$$

$$\mathcal{C} := [C, [C_{\Delta,k}]_{k \in \mathbb{N}_E}]. \quad (35)$$

Following [11], the gradient of the objective function J_R in (21) is determined as

$$\left. \frac{\partial J_R}{\partial i^{e*}} \right|_{i^{e*}=i^{e*(l)}} = (1 - \gamma)2B_2^\top L B_1 + 2\gamma \mathcal{D}(i^{e*(l)} - i^{eD}), \quad (36)$$

where, $\mathcal{D} := \text{diag}(\beta_k)_{k \in \mathbb{N}_E}$ and $L \geq 0$ is the solution of the Lyapunov equation

$$L\mathcal{A} + \mathcal{A}^\top L + \mathcal{C}^\top \mathcal{C} = 0. \quad (37)$$

Detailed derivations are given in the Appendix. After obtaining the gradient, the parameter of interest i^{e*} is updated as

$$i^{e*(l+1)} = i^{e*(l)} - \alpha_s \left. \frac{\partial J_R}{\partial i^{e*}} \right|_{i^{e*}=i^{e*(l)}}, \quad (38)$$

where, $\alpha_s > 0$ is the learning rate of the gradient, and l is the iteration number. To find the optimal value of α_s the traditional Armijo-rule-based line search is utilized which guarantees finite iteration convergence of (21)-(25) to a local optimum or the boundary of the constraint set. The steps for solving (21)-(25) are summarized in Algorithm 1.

C. Problem 2- Generalized EVCS integrated grid

In the previous section, we assumed that EVs only *consume* energy from the grid. However, at times of the day when the non-EV loads in the grid are high, and thereby the voltage stability margins may be low (for instance, connecting multiple EVs working in G2V mode to the end of a distribution line adversely affects its voltage profile, as shown in Fig. 3c), EVs can also be used to *supply* energy to the grid in exchange of a fee, and help in recovering voltage stability. In other words, integrating the EVCSs with bidirectional capacity operating on vehicle-to-grid (V2G) mode can be an effective solution to maintain desired voltage profiles in the grid. In this section, we assess the impacts of unidirectional and bidirectional EVCSs on the charging control and incentivization problem of our

Algorithm 1: Algorithm for joint parametric optimization and optimal control (21)-(26)

Input: $Q \geq 0, R > 0, \gamma \in [0, 1], l \leftarrow 1, i^{e*(1)}, i^{eD}, \epsilon > 0, \tau > 0, \underline{z}_k^{e*}$, and β_k for $k \in \mathbb{N}_E$

- 1 **while** $l \geq 2$ **and** $\|i^{e*(l+1)} - i^{e*(l)}\| \geq \tau$ **do**
- 2 Construct $A(i^{e*(l)}), B(i^{e*(l)})$, and \hat{x}_0 in (20). Compute $K(i^{e*(l)})$ by (24), $A_{cl}(i^{e*(l)})$ by (26), and $G_{i^{e*(l)}}(s)$ by (27)
- 3 **for** $k \in \mathbb{N}_E$ **do**
- 4 Compute ΔG_k in (30). Let its system matrices be $\{A_{\Delta,k}, B_{\Delta,k}, C_{\Delta,k}\}$.
- 5 Define \mathcal{A}, B_1, B_2 , and \mathcal{C} in (32)-(35)
- 6 Compute the gradient of J_R using (36)-(37)
- 7 Find optimal α_s using line search
- 8 Compute $i^{e*(l+1)}$ by (38)
- 9 Check if $i_k^{e*(l+1)}$ satisfy (19) and update for $k \in \mathbb{N}_E$, otherwise set to \underline{z}_k^{e*}
- 10 Let $l \leftarrow l + 1$

Output: converged $i^{e*(l)}, K$

interest integrated with voltage stability analysis using the VSI defined in (14).

Let $\mathbb{N}_{E_{uni}}$ and $\mathbb{N}_{E_{bi}}$ denote the set of buses corresponding to uni- and bi-directional EVCSs, i.e., $\mathbb{N}_{E_{uni}} \cup \mathbb{N}_{E_{bi}} = \mathbb{N}_E$ and $\mathbb{N}_{E_{uni}} \cap \mathbb{N}_{E_{bi}} = \emptyset$. Similar to in section IV-A, we consider that the EV owners demand i^{eD} as their charging rate, but the CPO offers i^{e*} as the rate instead to improve the system's SSI in exchange of an incentive. In addition, the CPO now also wants to improve the VSI by buying power from the EVs using their bidirectional chargers, and, therefore, has to pay a certain fee to the corresponding EV owners. If the total spending budget of the CPO is fixed, this would lead to a compromise between improving the SSI versus the VSI. We formulate this as an optimization problem by modifying the problem statement in (15)-(19) as follows:

$$J' = \min_{K, i^{e*}} (1 - \gamma_1 - \gamma_2) \underbrace{\int_0^\infty \|\hat{z}\|_2^2 dt}_{J_1} + \gamma_1 \underbrace{\|i^{e*} - i^{eD}\|_{2, \beta^{ip}}^2}_{J_2} + \gamma_2 \underbrace{\|\mathbf{1}_n - \mathcal{V}(i^{e*})\|_{\infty, \beta^{si}}}_{J_3} \quad (39)$$

$$\text{s.t. (13), (17), (18)} \quad (40)$$

$$i_k^{e*} \in [\max\{\underline{z}_k^{e*}, 0\}, i_k^{eD}], \quad k \in \mathbb{N}_{E_{uni}} \quad (41)$$

$$i_k^{e*} \in [\underline{z}_k^{e*}, i_k^{eD}], \quad k \in \mathbb{N}_{E_{bi}} \quad (42)$$

where, $\gamma_1, \gamma_2 \in [0, 1]$ are weighting constants that decide the priorities between SSI, VSI, and incentivization, β_k^{ip} and β_k^{si} are the price coefficients for $k \in \mathbb{N}_E$, $\mathcal{V} := [\mathcal{V}_2, \dots, \mathcal{V}_n]^\top \in \mathbb{R}^{n-1}$ with \mathcal{V}_h as defined in (14). The VSI is included in the term J_3 .

D. Solution Strategy of Problem 2

Similarly to Section IV-B, we consider

$$J'_R = \min_{i^{e*}} (1 - \gamma_1 - \gamma_2) \underbrace{\|G_{i^{e*}}\|_{\mathcal{H}_2}^2}_{J_{R1}} + \gamma_1 \underbrace{\|i^{e*} - i^{eD}\|_{2, \beta^{ip}}^2}_{J_{R2}}$$

$$+ \gamma_2 \underbrace{\|\mathbf{1}_n - \mathcal{V}(i^{e*})\|_{\infty, \beta^{si}}}_{J'_{R3}} \quad (43)$$

$$\text{s.t. (41), (42), (23), (24)} \quad (44)$$

where $G_{i^{e*}}$ is defined in (27). Similarly to (36), the gradient of J'_{R1} , and J'_{R2} are determined as

$$\left. \frac{\partial J'_{R1}}{\partial i^{e*}} \right|_{i^{e*}=i^{e*(l)}} = 2\mathcal{B}_2^\top L\mathcal{B}_1, \quad \left. \frac{\partial J'_{R2}}{\partial i^{e*}} \right|_{i^{e*}=i^{e*(l)}} = 2\mathcal{D}^{ip}(i^{e*} - i^{eD}), \quad (45)$$

where $\mathcal{D}^{ip} := \text{diag}(\beta_k^{ip})_{k \in \mathbb{N}_E}$. We next show how to obtain the gradient of J'_{R3} .

Due to the complicated nonlinearity of $J'_{R3}(i^{e*})$ to i^{e*} , we consider taking a numerical approximant of the gradient. Let $\mathbb{N}_E = \{k_1, \dots, k_p\}$, $\epsilon > 0$, p_k and e_k^p in (28). Under this setting, for $k \in \mathbb{N}_E$ the p_k -th element of the gradient is expressed as

$$\left[\frac{\partial J'_{R3}}{\partial i^e} \right]_{i^{e*}=i^{e*(l)}} \Big|_k \approx \frac{J'_{R3}(i^{e*(l)} + e_k^p \epsilon) - J'_{R3}(i^{e*(l)})}{\epsilon}. \quad (46)$$

By repeating this procedure for $k \in \mathbb{N}_E$, we can obtain a numerical approximant of $\partial J'_{R3}/\partial i^{e*}$. The overall gradient of J'_R can be approximated as

$$\hat{\nabla} J'_R := (1 - \gamma_1 - \gamma_2)2\mathcal{B}_2^\top L\mathcal{B}_1 + \gamma_1 2\mathcal{D}^{ip}(i^{e*(l)} - i^{eD}) - \gamma_2 \left[\frac{J'_{R3}(i^{e*(l)} + e_k^p \epsilon) - J'_{R3}(i^{e*(l)})}{\epsilon} \right]_{k \in \mathbb{N}_E}. \quad (47)$$

The optimization variable i^{e*} is then updated as

$$i^{e*(l+1)} = i^{e*(l)} - \alpha_v \hat{\nabla} J'_R, \quad (48)$$

where, α_v is the learning rate of the gradient, and l is the iteration number. To find the optimal value of α_v the traditional Armijo-rule-based line search can be utilized. The entire procedure is summarized in Algorithm 2.

Algorithm 2: Algorithm for joint optimization and optimal control design (39)-(42)

Input: $Q \geq 0$, $R > 0$, $\gamma_1, \gamma_2 \in [0, 1]$, $l \leftarrow 1$, $i^{e*(1)} i^{eD}$, $\epsilon > 0$, $\tau > 0$, \underline{i}_k^e , β_k^{ip} , β_k^{si} for $k \in \mathbb{N}_E$

- 1 **while** $l \geq 2$ **and** $\|i^{e*(l+1)} - i^{e*(l)}\| \geq \tau$ **do**
- 2 Construct $A(i^{e*(l)})$, $B(i^{e*(l)})$, and \hat{x}_0 in (20). Compute $K(i^{e*(l)})$ by (24), $A_{cl}(i^{e*(l)})$ by (26), and $G_{i^{e*(l)}}(s)$ by (27)
- 3 **for** $k \in \mathbb{N}_E$ **do**
- 4 Compute ΔG_k in (30). Let its system matrices be $\{A_{\Delta,k}, B_{\Delta,k}, C_{\Delta,k}\}$.
- 5 Define \mathcal{A} , \mathcal{B}_1 , \mathcal{B}_2 , and \mathcal{C} in (32)-(35)
- 6 Compute the gradients of J'_{R1} and J'_{R2} using (45)
- 7 Import network load (s) and line (t) data and define EVCS bus index $\mathbb{N}_{E_{\text{uni}}}$, and $\mathbb{N}_{E_{\text{bi}}}$
- 8 Compute \mathcal{V}_k for $k \in \{2, \dots, n\}$ using (14), and $\mathcal{V} := [\mathcal{V}_2, \dots, \mathcal{V}_n]^\top$.
- 9 Compute the gradient of J'_{R3} using (46)
- 10 Find optimal α_v using line search
- 11 Compute overall gradient of J'_R using (47)
- 12 Update, $i^{e*(l+1)}$ using (48)
- 13 Check if $i_k^{e*(l+1)}$ satisfy constraints (41)-(42) and update for $k \in \mathbb{N}_E$, otherwise set to \underline{i}_k^e
- 14 Let $l \leftarrow l + 1$

Output: converged $i^{e*(l)}$, K

V. PRACTICAL IMPLEMENTATION

We next state the set of actions that the CPO and the EV owners need to take once the CPO runs Algorithm 1 or 2 in practice. On the day before charging, the EV owners submit information about their charging energy demand as well as their desired power rate demand, which in most current fast-charging or discharging EVCSs come in the form of discrete levels such as 50 kW, 75 kW, and 150 kW [7]. Using this information, the CPO constructs the vectors $E^D := [E_k^D]_{k \in \mathbb{N}_E}^\top \in \mathbb{R}^p$, and $P^{eD} := [P_k^{eD}]_{k \in \mathbb{N}_E}^\top \in \mathbb{R}^p$, and computes the charging or discharging current demand vectors using $i^{eD} := P^{eD} \odot v^{dc*} \in \mathbb{R}^p$, where, $v^{dc*} := [v_k^{dc*}]_{k \in \mathbb{N}_E}^\top$ and v_k^{dc*} is the setpoint of v_k^{dc} defined in (8). For V2G mode, the sign of the charging power rate or charging current rate is considered to be negative, which is the opposite to the G2V mode. Using the chosen pricing co-efficient β (in Problem 1) or β^{si} , and β^{ip} (in problem 2), the CPO runs Algorithm 1 or 2 to determine the optimal charging current i^{e*} , and therefore, the optimal charging power rates $P^{e*} := i^{e*} \odot v^{dc*} \in \mathbb{R}^p$. Additionally, the CPO will estimate the charging duration (in minutes) at the demanded charging rate or contracted discharging rate as $C^{tD} := 60E^D \odot P^{eD} \in \mathbb{R}^p$. Similarly, the charging or discharging duration at the optimal charging or discharging rate vector is calculated as $C^{t*} := 60E^D \odot P^{e*} \in \mathbb{R}^p$. The charging price at the demanded charging or contracted discharging rate is calculated as $C^{PD} := E^D \odot \beta$. Based on this, the waiting time (in minutes), the dollar incentive, and the final charging cost are respectively calculated as $\mathcal{W}^t := C^{t*} - C^{tD}$, $\mathcal{I}^e := (C^{PD} \odot \mathcal{W}^t) \odot C^{tD}$ and $C^{P*} := C^{PD} - \mathcal{I}^e$, respectively.

The incentive offer is designed using a “wait & save” strategy, similar to the protocols used for ride-sharing applications e.g. Lyft [12]. This information can be integrated into a mobile app, enabling direct communication between the CPO and EV owners. EV owners using the mobile app can access the recommended offers provided by the CPO, and have the freedom to respond with their decisions.

Remark 1: Ideally, if any EV user rejects the incentivization offer, the CPO should re-optimize the remaining setpoints to still guarantee the minimum value of J_R in (21) or J'_R in (43), and the new values of the waiting times and incentives should be communicated to the users who accepted their offers in the previous round. The user has the option of accepting or rejecting this new offer, based on which the CPO may need to re-optimize again. This negotiation can continue to the app until a consensus of acceptance or rejection is reached. For the sake of brevity, we skip this re-optimization scenario in this paper and reserve it for our future work.

VI. NUMERICAL RESULTS

We validate our proposed method using the IEEE 33-bus power distribution radial feeder model. This model has an operating voltage of 12.66 kV, has 33 buses, and supports a 3.715 MW non-EV load. Traditional PI controller-based EVCSs are used with the dynamic model and power flow balance listed in Section II. We have seen in Fig. 3 that the damping worsens as the number of EVCSs increases. We aim to improve these damping factors using the co-design of K

and i^{e*} , as stated in Algorithm 1 or K , and i^{e*} in Algorithm 2. To simplify the design, we eliminate the fast states of the model and perform a model reduction via singular perturbation [13]. The rest of the design results are explained as follows.

A. Simplified EVCSs integrated grid

1) *Single Port EVCSs*: Let us consider a charging scenario on any given day, where $p = 6$ EVs with the same battery capacity (75 KWhr, 360V) submit the same charging demand $E^D = 451_p$ KWhr i.e. 60% of its capacity. We assume $p = 3$ EVCSs case in Section III, i.e., $\mathbb{N}_E = \{3, 19, 5\}$, each containing a single charging port. The customer-demanded charging power rates at those three EVCSs are $P^{eD} = [50, 50, 100]^T$ kW, and corresponding charging current demands are $i^{eD} = [62.5, 62.5, 125]^T$ A, considering $v^{dc*} = [800, 800, 800]^T$ V. With this submitted information, the CPO applies Algorithm 1, and divides the six EV loads equally among the three EVCSs, where, each EVCS accommodates two EVs sequentially with no intervals of inactivity. To represent EV arrivals and departures in a condensed time frame under the state-of-charge (SOC) requirement, a scale-down of the demand needs to be done. We have scaled down the required 45 KWhr demand to 0.04 KWhr (scale-down ratio of 1/1050), and accordingly, the charging duration for the 50 kW and 100 kW chargers is reduced from their actual magnitudes of 54 minutes and 27 minutes to 2.8s and 1.4s of simulation time, respectively.

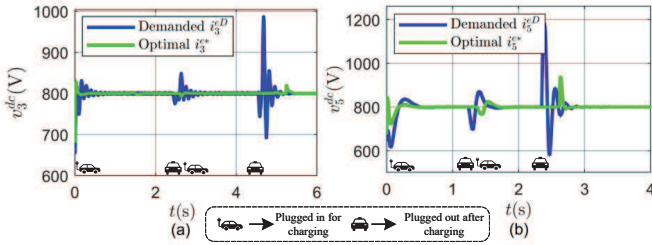


Fig. 4. Comparison of DC bus voltage response with (a) $i_3^{eD} = 62.5$ A, and $i_3^{e*} = 56.44$ A, and (b) $i_5^{eD} = 125$ A, and $i_5^{e*} = 116.53$ A

With $\gamma = 0$, Algorithm 1 yields the following optimal solutions: $i_3^{e*} = 55.97$ A, $i_{19}^{e*} = 56.03$ A, and $i_5^{e*} = 115.84$ A for the respective EVCSs with corresponding charging power rates $P_3^{e*} = 44.77$ kW, $P_{19}^{e*} = 44.82$ kW, and $P_5^{e*} = 92.67$ kW, respectively. The optimization reduces the \mathcal{H}_2 -norm of the system transfer function $G_{i_e^*}(s)$ in (27) from 0.0015 to 5.932×10^{-4} . We apply the state-feedback controller K and the optimal setpoints i^{e*} in the original nonlinear model (13) of the 33-bus system, and consider a disturbance response due to the sudden connection of the EVs. Fig. 4 shows the converter state responses (specifically, the DC bus voltage v^{dc}) for this charging scenario. Note that the voltage ripple in v^{dc} depends on the current drawn. Therefore, the conventional PI-based model with the demanded i^{eD} faces a higher risk of sustained voltage oscillations due to sudden plug-ins of the high-power EV loads. This is also indicated in the voltage tolerance curves that are shown in [14].

A single figure is shown for the first two 50 kW charging stations as their capacities and optimization results are quite similar. Figure 4 clearly illustrates that reducing the \mathcal{H}_2 -norm

leads to a significant improvement in transient response, as compared to the conventional PI-based controller with demand i^{eD} . The algorithm initially suggests a charging rate that is much lower than the customer's demand, potentially discouraging the customer's choice to use the EVCS. To address this, we introduce the incentivization term J_{R2} in (21) that can be utilized by the CPO to ensure customer participation via a proper incentive. The CPO can tune the weighting factor γ to attract EV customers. $\gamma = 0$ prioritizes system dynamics over customer satisfaction, reducing the \mathcal{H}_2 -norm from 0.0015 to 5.932×10^{-4} , while suggesting sub-demand charging currents. As γ increases, both parts of the objective functions gain priority, leading to a trade-off. As γ approaches 1, emphasizing customer satisfaction over grid health, the algorithm suggests the use of charging currents that are closer to the customer demand but at the expense of degraded transient response of the grid states.

2) *Multi-port EVCSs*: Moving beyond single charging port, we next study the impact of multi-port EVCSs on the closed-loop response. We consider the same three EVCSs in the 33-bus radial network, but now the first two EVCSs contain four charging ports each, and the third EVCS contains a single charging port. The charging rates for the first two EVCSs are 50 kW each, and that for the third EVCS is 100 kW. We assume the CPO allocates the first four EVs to EVCS-1 and the remaining two to EVCS-3. Considering the condensed time frame, EV 1 joins the first charging port at EVCS-1 at $t = 1$ s, and leaves at $t = 20.7$ s after receiving its 45 KWhr of charging demand (i.e. 60% of total SOC level of 75 KWhr). The other EVs join and leave their respective charging ports while EV 1 is charging at charging port 1 of EVCS-1. The transient response for the single charging port of EVCS-3 is found to be similar to that in Fig. 4 (b), and therefore, is not repeated here. The responses for the other ports are shown in Fig. 5 using Algorithm 1, for $\gamma = 0$ and $\gamma = 0.5$. As expected, the transient response is best for $\gamma = 0$ while the charging current is lower than the demand. The transient response worsens with increasing γ while the CPO saves money by bringing the charging current closer to the demand.

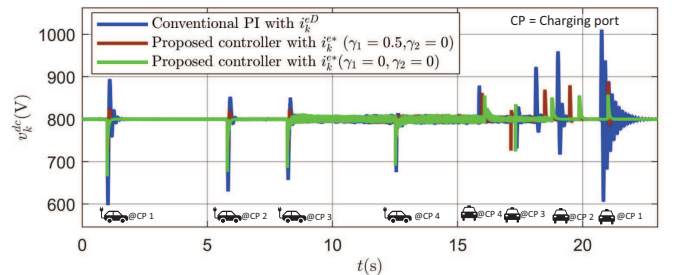


Fig. 5. Comparison of DC bus voltage considering multi-port EVCSs. Here, the multi-port EVCS contains 4 charging ports (CPs), where EVs are plugged in and out at different times.

3) *Negotiation through Incentivization*: For each $k \in \mathbb{N}_E$, we set $\beta_k = 0.4$ /KWhr during off-peak and $\beta_k = 0.5$ /KWhr during peak hours (for charging power rates under 50 kW), and $\beta_k = 0.5$ /KWhr during off-peak and $\beta_k = 0.6$ /KWhr during

TABLE IV
DATA TABLE FOR NEGOTIATION BETWEEN CPO AND EV OWNER WHILE UTILIZING THE PROPOSED INCENTIVIZATION STRATEGY

Cases	EVCS ID	CPO Side				Customer Side (Mobile App)				Grid VSI Monitoring		
		E^D	P^{eD}	P^{e*}	Decision	C^{t*}, C^{tD}	\mathcal{W}^t	\mathcal{I}^e	$C^{\mathcal{P}*}, C^{\mathcal{P}D}$	\mathcal{V}^D	\mathcal{V}^S	\mathcal{V}^B
1	EVCS-1	45	50	45	✓	60	6	2	16	-	0.9324	0.936
					×	54	0	0	18	0.9316	-	
	EVCS-3	45	100	90.8	✓	29.7	2.7	2.25	20.25	-	0.874	0.884
					×	27	0	0	22.5	0.8729	-	
	EVCS-5	45	150	139	✓	19.4	1.4	1.75	20.75	-	0.8001	0.810
					×	18	0	0	22.5	0.7988	-	
2	EVCS-1	45	30	25.5	✓	106	16	4	18.5	-	0.9341	0.936
					×	90	0	0	22.5	0.9328	-	
	EVCS-3	45	75	67.1	✓	40.2	4.2	3.2	23.8	-	0.8768	0.884
					×	36	0	0	23.8	0.8754	-	
	EVCS-5	45	120	107.4	✓	25.1	2.6	3.1	23.9	-	0.8027	0.810
					×	22.5	0	0	27	0.8015	-	

EV owner decision: ✓ =Accept, × =Reject. Unit: $C^{tD}, C^{t*}, \mathcal{W}^t$ in minutes, E^D in KWhr, P^{eD}, P^{e*} in kW, and $\mathcal{I}^e, C^{\mathcal{P}D}, C^{\mathcal{P}*}$ in \$.

peak hours (for charging rates exceeding 50 kW), based on average prices from US charging providers [15]. We assume $p = 3$ EVCSs connected to buses 3, 5, and 15, i.e., $\mathbb{N}_E := \{3, 5, 15\}$, each with a charging energy demand of 45 KWhr, as shown in Table IV. Here, the EVCS ID is the corresponding serial number of the EVCSs as shown in Fig. 2. The optimal charging power rates P^{e*} from Algorithm 1 are lower than P^{eD} , extending the charging duration C^{tD} (Section IV). We introduce the "wait & save" strategy [12], where EV customers trade a brief waiting time \mathcal{W}^t for saving money, reducing their final charging price $C^{\mathcal{P}*}$. To explain this, we consider two cases: Case-1, EV charging loads in the mentioned EVCSs with three different demands P^{eD} in off-peak, and Case-2, EV charging loads with lower demands P^{eD} in peak hours.

The corresponding data log observed from the CPO side and on the mobile app screen of the customer side are shown in Table IV. Additionally, the VSI at the EVCS buses, i.e. $k \in \mathbb{N}_E$ is computed following [16], and tabulated in Table IV, where, the base load VSI (i.e. with no EV load at EVCS buses) is denoted as \mathcal{V}^B at $k \in \mathbb{N}_L$. In case 1, three EV loads join at the three EVCS buses with P^{eD} of 50 kW, 100 kW, and 150 kW, respectively. Thereafter, the CPO runs Algorithm 1, and determines the optimal P^{e*} as 45 kW, 90.8 kW, and 139 kW, respectively. Therefore, the charging durations C^{t*} become 60 minutes, 29.7 minutes, and 19.4 minutes, respectively. The charging durations C^{tD} if the EVs stick to their demanded power, however, are 54 minutes, 27 minutes, and 18 minutes, respectively. The respective customers, therefore, will have to wait for an extra 6 minutes, 2.7 minutes, and 1.4 minutes, which eventually saves them \$2, \$2.25, and \$1.75 as incentives \mathcal{I}^e (calculated based on the equivalent dollar value for staying the extra time), helping to reduce their final charging price $C^{\mathcal{P}*}$. The utilization of lower P^{e*} also slightly improves the VSI than P^{eD} , as shown in Table IV, where \mathcal{V}^S is the VSI when the customer agrees to go with optimal charging rate, and \mathcal{V}^D is the VSI when they reject the idea of the optimal rate and prefer to stick to their demand. The same observation is found for case 2, as shown in Table IV.

More importantly, the optimal rate helps in improving the damping performance of the grid states, as expected from Algorithm 1. The closed-loop eigenvalue plots for cases 1 & 2, and the respective transient responses of the DC bus voltage

(considering the mentioned shorter time frame) are shown in Figs. 6 and 7, respectively. It is seen that the system response is significantly better if the consumer accepts the proposed charging rate. If the consumer rejects the suggested charging rate, the closed-loop response degrades but remains better than that for the demanded charging rates. In summary, the proposed dynamics-aware charging scheme provides beneficial returns for both the grid operator and the EV customers but remains a concern on voltage stability that can be overcome by utilizing both the G2V and V2G mode simultaneously which is discussed in the next subsection.

B. Generalized EVCSs integrated grid

For validating Problem 2, we consider the same IEEE 33 bus model as shown in Fig. 2 with $p = 10$ EVCSs, where 7 EVCSs connected at buses 3, 5, 9, 19, 21, 26, and 32 are considered to be operating in uni-directional G2V mode, and 3 EVCSs at buses 11, 15, and 17 are assumed to operate as bi-directional EVCSs. The nominal VSI without any EVCS in the network (as shown in Fig. 3c) is found to be the lowest at bus 18 with a value of 0.7141. This VSI is marked as \mathcal{V}_{\min} . Due to the radial nature of the network, it can be easily seen that the VSIs at all other buses will improve, in general, if \mathcal{V}_{\min} improves. We consider that two EVs in each EVCS with the same battery capacity (120 KWhr, 360V) submit their charging demand as 90 KWhr, due to which the VSI of the critical bus reduces to $\mathcal{V}_{\min} = 0.5768$. The CPO, therefore, decides to purchase power from the EVCSs that have bi-directional capabilities. The demanded charging and contracted discharging rates, denoted as P^{eD} , are shown in Table V. The bracketed sign indicates the EVCSs that operate in V2G mode only. Given this submitted demand information, the CPO runs a power flow program and obtains the critical VSI (without applying Algorithm 2) as $\mathcal{V}_{\min} = 0.654$, indicating an improvement in voltage due to the added energy supplied by the EVCSs. However, the SSI is still sub-optimal as the charging/discharging current setpoints are not optimized. The CPO, therefore, runs Algorithm 2 to co-optimize SSI, VSI, and the incentives.

The results from Algorithm 2 are presented in Table V. For Case 1, we assume $\gamma_1 = \gamma_2 = 0$, giving higher priority to SSI. In this case, the algorithm provides lower charging

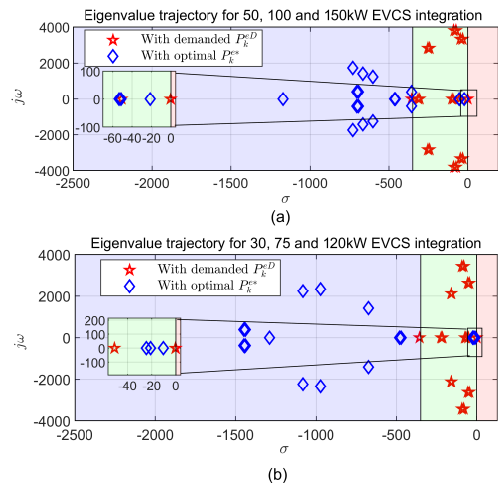


Fig. 6. Eigenvalue plots showing improvement of closed-loop damping factors for the dominant poles for cases 1 and 2 of Table IV.

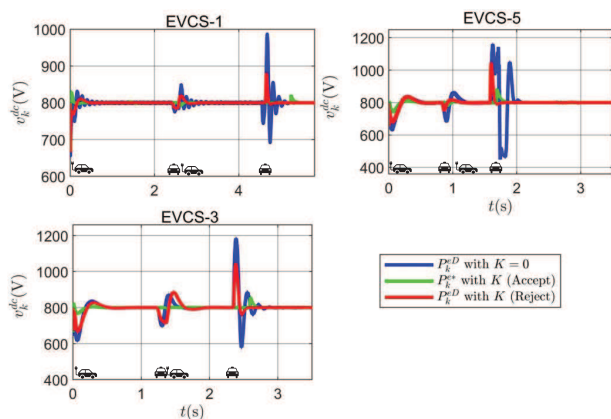


Fig. 7. The DC bus voltages of all EVCSs in case 1 of Table IV.

and discharging power rates, denoted as P^{e*} in the table for the corresponding EVCSs, ensuring lower SSI with a \mathcal{H}_2 -norm of 9.65×10^{-4} . The optimal results also ensure an improvement in VSI (i.e., 0.630) from the unidirectional non-optimal case (i.e., 0.5768). However, this costs the CPO an incentive of \$51.47. In case 3, the CPO aims to reduce the incentive and give more priority to the VSI improvement by setting $\gamma_1 = 0$ and $\gamma_2 = 0.6$. The algorithm provides a slightly higher power rate by sacrificing the SSI from 9.65×10^{-4} to 1.6×10^{-3} , but ensures a lower incentive of \$37.13 and a higher VSI of 0.770. In case 2, equal priority is given to SSI improvement, customer satisfaction, and VSI improvement. For this case, the charging and discharging power rates are closer to the customer demand, which reduces the incentive cost, but the SSI and VSI are both reduced from their nominal values. The trends of the VSI and the bus voltages using Algorithm 2 for the above three cases are shown in Fig. 8c. The figure indicates how the CPO may decide on the interplay between the three objectives in (39) to ensure a balance between the grid health, EV customer satisfaction, and total expenditure. The time-domain responses of the DC bus voltages for selected EVCSs are shown in Fig. 8b. For

TABLE V
DATALOG FOR THE CONSIDERED EVCS INTEGRATED NETWORKS WITH BIDIRECTIONAL CAPABILITY IN DIFFERENT CASES.

EVCS	P^{eD}	P^{e*}	\mathcal{W}^t	\mathcal{I}^e	$\sum \mathcal{I}^e$	$\ G_{ie}\ _{\mathcal{H}_2}^2$	\mathcal{V}_{\min}
Case 1: $\gamma_1 = 0, \gamma_2 = 0$							
1	50	42.5	19.06	6.35	51.47	$9.65e-4$	0.630
2	100	85	9.53	7.94			
3	100	86.85	8.18	6.82			
4	(175)	(164.88)	1.89	2.75			
5	(150)	(143.15)	1.72	2.15			
6	(175)	(169.83)	0.94	1.37			
7	50	42.5	19.06	6.35			
8	100	85.94	8.83	7.36			
9	50	42.5	19.06	6.35			
10	100	91.77	4.84	4.03			
Case 2: $\gamma_1 = 0.33, \gamma_2 = 0.33$							
1	50	45.87	9.72	3.24	19.37	$1.5e-3$	0.691
2	100	94.83	2.94	2.45			
3	100	95.91	2.30	1.92			
4	(175)	(171.83)	0.55	0.80			
5	(150)	(147.84)	0.53	0.66			
6	(175)	(173.38)	0.29	0.42			
7	50	44.98	12.05	4.02			
8	100	95.63	2.47	2.06			
9	50	46.63	7.81	2.60			
10	100	97.42	1.43	1.20			
Case 3: $\gamma_1 = 0, \gamma_2 = 0.6$							
1	50	42.75	18.32	6.10	37.13	$1.6e-3$	0.770
2	100	92.11	4.63	3.86			
3	100	92.73	4.23	3.53			
4	(175)	(168.38)	1.21	1.76			
5	(150)	(144.11)	1.47	1.84			
6	(175)	(169.45)	1.01	1.47			
7	50	42.5	19.06	6.35			
8	100	92.53	4.36	3.63			
9	50	43.24	16.88	5.63			
10	100	93.81	3.56	2.96			

Case 1, where $\gamma_1 = 0 = \gamma_2 = 0$, the transient response of the bus voltage is significantly better than the other cases. The eigenvalue shift shown in Fig. 8a also suggests the improvement of SSI. For Case 3, the SSI is reduced at the expense of maximizing the VSI and reducing the incentive. The DC bus voltage responses show this degradation, with the corresponding closed-loop eigenvalues marked as green boxes in Fig. 8a moving closer to the imaginary axis. A similar and consistent observation is made for case 2 as well.

VII. CONCLUSIONS

We presented a joint optimization and optimal control design for charging control of EVs in power distribution networks that benefit the grid operator by improving the small-signal damping performance of the grid states, and also the EV owners by providing them financial incentives in exchange for slightly higher waiting times than what they intended. The damping improvement is achieved by a joint LQR state-feedback design for the charging current and by reducing the \mathcal{H}_2 -norm of the system transfer function by finding the optimal setpoints for these charging currents. Both unidirectional and bidirectional charging scenarios are considered. The latter is seen to bring out interesting trade-offs between small-signal stability, voltage stability, and incentivization. The proposed approach is validated using simulations on a benchmark distribution grid, showcasing their effectiveness in mitigating voltage oscillations as well as in optimizing the charging costs of EVs. Our future work will include extending this optimization approach to the temporal scheduling of EVs, considering human behavioral factors and demand response.

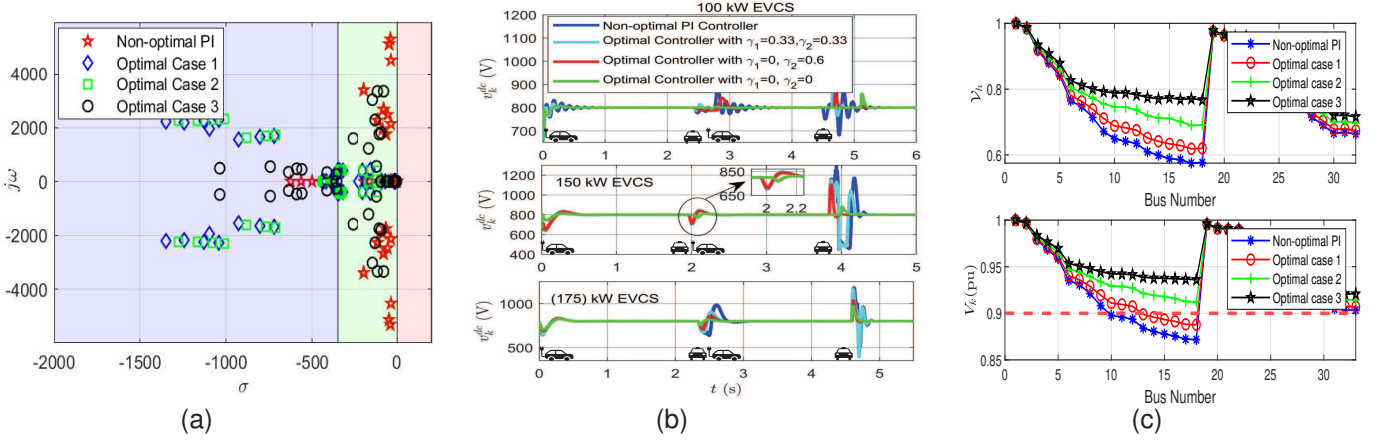


Fig. 8. (a) Eigenvalue trajectory of the non-optimal PI controller, and three cases of Table VI. Noted that case 1: $\gamma_1 = 0, \gamma_2 = 0$, case 2: $\gamma_1 = 0, \gamma_2 = 0.6$, and case 3 $\gamma_1 = 0.33, \gamma_2 = 0.33$ with the proposed optimal controller, (b) The DC bus voltages of all cases of Table VI and the non-optimal PI-based controller, which provides the time-domain aspect of the system response, and (c) Trends of VSI values with the application non-optimal PI control and the proposed optimal controller with different weighting factors.

APPENDIX

A. EVCS Parameters

The parameters during the design of the 50kW EVCS are summarized as follows: For any $k \in \mathbb{N}_E$, $L_k^g = L_k^c = 2mH$, $C_k^f = 30\mu F$, $v_k^{dc} = 800V$, $\kappa_k^{P1} = 1.71$, $\kappa_k^{I1} = 672.66$, $\kappa_k^{P2} = 0.5$, $\kappa_k^{I2} = 5$, $\kappa_k^{P3} = 25$, $\kappa_k^{I3} = 500$, $\kappa_k^{P4} = 25$, $\kappa_k^{I4} = 500$, $C_k^{dc} = 5600\mu F$.

B. Derivation for determining the gradient of J_R in (21)

Following [11], the gradient of J_{R1} part of J_R can be expressed as:

$$\begin{aligned} J_{R1} &= \|G_{i^{e*}}\|_{\mathcal{H}_2}^2 = \text{tr}(\mathcal{B}^\top L \mathcal{B}) \\ &= \text{tr}\left((\mathcal{B}_1 + \mathcal{B}_2 \epsilon \mathbf{1}_p)^\top L (\mathcal{B}_1 + \mathcal{B}_2 \epsilon \mathbf{1}_p)\right) \\ &\implies \left. \frac{\partial J_{R1}}{\partial i^{e*}} \right|_{i^{e*}=i^{e*(t)}} = 2\mathcal{B}_2^\top L \mathcal{B}_1. \end{aligned} \quad (49)$$

Similarly, the gradient of J_{R2} in (21) can be derived as:

$$\begin{aligned} J_{R2} &= \|\hat{i}^{e*(t)} + \bar{i}^{e*}\|_{2,\beta}^2 = (\hat{i}^{e*(t)} + \bar{i}^{e*})^\top \mathcal{D} (\hat{i}^{e*(t)} + \bar{i}^{e*}) \\ &= \mathcal{D} \hat{i}^{e*(t)\top} \bar{i}^{e*} + 2\mathcal{D} \bar{i}^{e*\top} \hat{i}^{e*(t)} + \mathcal{D} \bar{i}^{e*\top} \bar{i}^{e*} \\ &\implies \left. \frac{\partial J_{R2}}{\partial i^{e*}} \right|_{i^{e*}=i^{e*(t)}} = 2\mathcal{D} (i^{e*(t)} - i^{eD}) \end{aligned} \quad (50)$$

where, $\hat{i}^{e*(t)} = (i^{e*(t)} + e_k^p \epsilon)$, $\bar{i}^{e*} = i^{e*(t)} - i^{eD}$.

REFERENCES

- [1] K. Qian, C. Zhou, M. Allan, and Y. Yuan, "Modeling of load demand due to EV battery charging in distribution systems," *IEEE Trans. Power Syst.*, vol. 26, no. 2, pp. 802–810, May 2011.
- [2] C. Le Floch, F. Belletti, and S. Moura, "Optimal charging of electric vehicles for load shaping: A dual-splitting framework with explicit convergence bounds," *IEEE Trans. Transport. Electrification*, vol. 2, no. 2, pp. 190–199, Jun. 2016.
- [3] Y. Xu, "Optimal distributed charging rate control of plug-in electric vehicles for demand management," *IEEE Trans. Power Syst.*, vol. 30, no. 3, pp. 1536–1545, May 2015.
- [4] I. S. Bayram, G. Michailidis, M. Devetsikiotis, and F. Granelli, "Electric power allocation in a network of fast charging stations," *IEEE J. Sel. Area Comm.*, vol. 31, no. 7, pp. 1235–1246, Jul. 2013.
- [5] W. Du, Q. Fu, and H. F. Wang, "Small-signal stability of a DC network planned for electric vehicle charging," *IEEE Trans. Smart Grid*, vol. 11, no. 5, pp. 3748–3762, Sep. 2020.
- [6] Q. Fu, W. Du, and H. Wang, "Planning of the DC system considering restrictions on the small-signal stability of EV charging stations and comparison between series and parallel connections," *IEEE Trans. Veh. Technol.*, vol. 69, no. 10, pp. 10724–10735, Jul. 2020.
- [7] M. M. Mahfouz and M. R. Iravani, "Grid-integration of battery-enabled DC fast charging station for electric vehicles," *IEEE Transactions on Energy Conversion*, vol. 35, no. 1, pp. 375–385, 2020.
- [8] N. Pogaku, M. Prodanovic, and T. C. Green, "Modeling, analysis and testing of autonomous operation of an inverter-based microgrid," *IEEE Trans. Power Electron.*, vol. 22, no. 2, pp. 613–625, 2007.
- [9] S. Sivakumar, S. B. Ramasamy Gunaseelan, M. V. Reddy Krishnakumar, N. Krishnan, A. Sharma, and A. Aguila Téllez, "Analysis of distribution systems in the presence of electric vehicles and optimal allocation of distributed generations considering power loss and voltage stability index," *IET Gener. Transm. Distrib.*, vol. 18, pp. 1114–1132, Sep. 2023.
- [10] A. Arancibia and K. Strunz, "Modeling of an electric vehicle charging station for fast dc charging," in *IEEE Int. Elect. Veh. Conf.*, Mar. 2012, pp. 1–6.
- [11] M. Inoue, T. Sadamoto, M. Arahata, and A. Chakraborty, "Optimal power flow design for enhancing dynamic performance: Potentials of reactive power," *IEEE Trans. Smart Grid*, vol. 12, no. 1, pp. 599–611, Jan. 2021.
- [12] L. Blog. (2020) Wait & save: The most affordable Lyft ride for households and individuals. Accessed on: August 05, 2023. [Online]. Available: <https://www.lyft.com/blog/posts/wait-and-save>
- [13] H. K. Khalil, *Nonlinear Systems*, 3rd ed. Upper Saddle River, NJ: Prentice Hall, December 2007.
- [14] D. Symanski and C. Watkins, "380VDC data center at duke energy," 2010.
- [15] M. Services. (2023) The average costs of using car charging stations. Accessed on: September 05, 2023. [Online]. Available: <https://www.mach1services.com/costs-of-using-car-charging-stations/>
- [16] M. Chakravorty and D. Das, "Voltage stability analysis of radial distribution networks," *Int. J. Elect. Power Energy Syst.*, vol. 23, no. 2, pp. 129–135, Feb. 2001.